Using Energy Landscapes To Predict the Properties of Thin Films[†]

Jeetain Mittal and Pooja Shah

Department of Chemical Engineering, The University of Texas at Austin, Austin, Texas 78712

Thomas M. Truskett*

Department of Chemical Engineering and Institute for Theoretical Chemistry,
The University of Texas at Austin, Austin, Texas 78712

We develop an energy landscape based mean-field theory for thin films confined between parallel substrates. We use the approach to explore how the dimensions of the film and the interactions between the film and the substrates impact the equilibrium phase diagram and the ideal glass transition. The theoretical predictions are in qualitative agreement with the experimentally observed trends for confined fluids. We also use the theory to determine how the average pressure tensor of minimum energy configurations (i.e., inherent structures) depends on film density. This is, to our knowledge, the first theoretical prediction of an "equation of state of an energy landscape" for thin films. It suggests how the intrinsic mechanical properties of thin-film glasses derive from the physical dimensions of the sample, the interactions between the film and the substrates, and the balance between internal cohesive and packing forces.

I. Introduction

Materials confined to nanoscale dimensions can display physical properties that are different from the corresponding bulk samples. In fact, limits of thermodynamic, kinetic, and mechanical stability for these systems such as phase boundaries, the glass transition temperature, and strains (or stresses) to failure are known to be particularly sensitive to both the degree and "type" of confinement.[1−10] In the case of thin films, two generic factors are known to play a central role: (i) the spatial dimensions of the film and (ii) the nature of the confining interfaces. However, the lack of a comprehensive molecular-level theory makes it difficult to predict the properties of thin films a priori, even if detailed information regarding the aforementioned factors is available.

This incomplete understanding not only poses outstanding scientific challenges but also represents a practical barrier to developing a host of technological applications. Examples include protective coatings for magnetic hard disks, multilayer nanocomposites, photoresist materials for semiconductor fabrication, and intermediate layers for mediating interface adhesion, bonding, or wetting in high-resolution printing or patterning applications.[7−10] Discovering, understanding, and elucidating the physical forces that determine the stability of solid (glassy or crystalline) nanostructures is of particular interest because most technological applications require components that exhibit mechanical integrity over a broad range of conditions.

One powerful tool for understanding the relationship between the physical properties, the structure, and the molecular interactions of materials is the potential energy landscape,[11,12] i.e., the hypersurface that the total potential energy of a system forms as a function of its configurational degrees of freedom. Though topographically complex, only a few statistical features of the landscape have been found to significantly influence the

thermodynamic, mechanical, and transport properties of condensed-phase systems. These include the properties of the minima at each given elevation, the shapes of the basins of attraction that surround the minima, and the details of the saddle-point barriers that separate neighboring basins.[13−16] Computational investigations of these properties for bulk systems have advanced our understanding of melting and freezing phenomena in 2D and 3D, the thermal and mechanical properties of glasses, and relaxation processes in supercooled liquids.[13,15]

In this Article, we explore how the potential energy landscape can provide insights into how the properties of a material will change when confined to a thin film. In particular, we present an energy landscape based mean-field theory that relates the anisotropic stresses in confined glassy materials to the sample dimensions, the physical interactions of the film with the confining substrates, and the balance between internal molecular packing and cohesive forces. We then use the theory to predict some possible thermal and mechanical limits for forming mechanically stable amorphous thin films. The specific film properties predicted by the theory include the ideal glass transition temperature, the mechanical properties of the minimum energy configurations (i.e., inherent structures), and the phase diagram.

The organization of the Article is as follows. In section II, we develop the landscape formalism and an analytical mean-field theory for a film confined between parallel substrates. In section III, we outline the main predictions of the theory. Finally, in section IV, we discuss the conclusions of our study and speculate on how some approximations invoked in the theory might be improved.

II. Theory and Model Development

Energy Landscape Formalism for Thin Films. We consider a collection of identical and structureless particles that constitute a film with dimensions $A \times L$, where A is the contact area

---

[†] Part of the special issue "Frank H. Stillinger Festschrift".
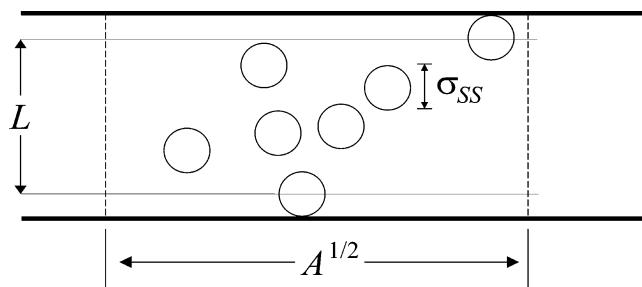* To whom correspondence should be addressed.

Figure 1. Schematic of a thin film of particles of diameter σ_{SS} with centers confined to a volume $V = AL$ by rigid and smooth parallel substrates.

Figure 2. Simplified 1D schematic of the multidimensional potential energy hypersurface exhibiting some of the features important for understanding the properties of condensed-phase systems. $\phi*$ is the average value of the potential energy minima of the basins that the system preferentially samples under a given set of equilibrium conditions. The ideal glass, if it exists, corresponds to the single deepest "amorphous" basin on the landscape.

between the film and one of the confining substrates and L is the film thickness (Figure 1). Experiments on systems of this sort, e.g., via the surface force apparatus, are commonly performed under conditions of constant temperature and chemical potential—variables naturally associated with the grand canonical ensemble. However, in the present analysis, it will be convenient to work in the canonical ensemble, where the independent variables are the film dimensions $\{A, L\}$, the number of film particles N, and temperature T. This choice is acceptable because we are focusing on the behavior of films in the thermodynamic limit (i.e., N, $A \to \infty$ with finite number density $\rho = N/AL$), where all statistical mechanical ensembles are equivalent and predict identical equilibrium properties. The canonical partition function Z_N for this system can be formally expressed

$$Z_N = \exp[-\beta N f] = (\lambda_T^{3N} N!)^{-1} \int \exp[-\beta \Phi(\mathbf{r}^N | \{A,L\})] \, d\mathbf{r}^N \tag{1}$$

where f is the Helmholtz free energy per particle, $\beta = 1/k_B T$ is the reciprocal temperature, and λ_T is the mean thermal deBroglie wavelength of the particles. The total potential energy is written as $\Phi(\mathbf{r}^N | \{A,L\})$ to indicate that it depends on the positions of the N particles $\mathbf{r}^N = \{r_1, r_2, ..., r_N\}$, which are confined to the physical dimensions of the film.

Obtaining an approximate analytical solution for the multidimensional integral of eq 1 is a formidable task, even for systems with relatively simple interparticle interactions. However, the potential energy landscape formalism of Stillinger and Weber[11] allows Z_N to be recast in an alternative form that has proven useful for analyzing the properties of bulk materials. Here, we explore how this landscape based approach can also be used to develop theories for the behavior of thin films.

The energy landscape referred to here is the hypersurface that the potential energy Φ forms in the $3N + 1$-dimensional space of Φ and $\mathbf{r}^N$, and it is illustrated schematically in Figure 2. The topographical features of the landscape are determined by the quantities that affect the relationship between Φ and $\mathbf{r}^N$: the total number of particles, the dimensions of the film, and the interparticle potentials of the film and the substrate. The formal connection between the energy landscape and the partition function (explored in detail elsewhere[15]) relies on an exhaustive division of configuration space into nonoverlapping basins or "valleys" that surround each local potential energy minimum. Here, a *basin* is defined to be the set of configurations that would map to the same structure under a steepest-descent energy minimization, and the particle packings that correspond to the local minima in Φ are called *inherent structures*. This type of configurational mapping, when applied to equilibrium liquid configurations, essentially corresponds to the physical process of rapidly cooling to a temperature far below the glass
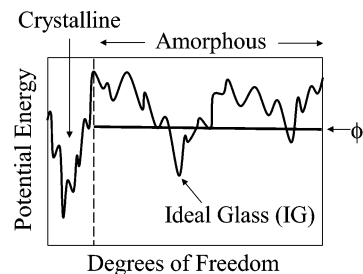
transition.[17] Hence, the amorphous inherent structures of a material are intimately connected to its glassy state.

The aforementioned partitioning of configuration space allows Z_N to be expressed as a sum of contributions from each basin on the energy landscape. To facilitate this description, it is convenient to classify the basins by "elevation", as measured by the potential energy per particle ϕ of their associated inherent structures. Condensed-phase materials generally exhibit a diverse set of inherent structures with substantial variation in ϕ, ranging from the deepest minimum on the landscape $\phi = \phi_{\min}(\rho, L)$ to the highest-lying minimum-energy configuration $\phi = \phi_{\max}(\rho, L)$. This diversity of basins makes the energy landscape "rugged", a feature that has important implications for the thermodynamic and kinetic behavior of supercooled liquids and the history-dependent properties of glasses[13,15]

The connection between basin statistics and equilibrium thermodynamics is made through the canonical partition function of eq 1, which can be recast as a one-dimensional integral over basin depth ϕ,[11,15]

$$Z_N = C \int_{\phi_{\min}(\rho,L)}^{\phi_{\max}(\rho,L)} \exp[-N\{\beta\phi - \sigma(\phi,\rho,L) + \beta f_{\text{vib}}(\phi,\beta,\rho,L)\}] \, d\phi \tag{2}$$

Here, $C\exp[N\sigma(\phi,\rho,L)]$ quantifies the probability density associated with finding basins of depth ϕ on the landscape, $\sigma(\phi,\rho,L)$ is called the *basin enumeration function*, and C is a normalization constant of dimension reciprocal energy. The function $\exp[-N\beta f_{\text{vib}}(\phi,\beta,\rho,L)]$ is an "intrabasin" partition function associated with the vibrational motion of the system's configuration point $\mathbf{r}^N$ inside basins of depth ϕ.

In the present context, we are interested in describing the behavior of amorphous (i.e., fluid and glassy) thin films. Thus, we define the functions σ, $\phi_{\min}$, $\phi_{\max}$, and f_{vib} of eq 2 so that they characterize only the basins containing particle configurations substantially devoid of crystallinity. This constraint on the type of basins that the configuration point can visit effectively seals off the pathways to crystal nucleation on the landscape,[18] and it allows eq 2 to describe supercooled liquid states that appear equilibrated on laboratory or simulation time scales.

The saddle point approximation provides the leading order contribution to the integral in eq 2, and it yields the following expression for the Helmholtz free energy f in the thermodynamic limit:

$$f = \phi* - \sigma(\phi*,\rho,L)/\beta + f_{\text{vib}}(\phi*,\beta,\rho,L) \tag{3}$$

Here, $\phi*$ characterizes the average depth of the basins that the

Predicting the Properties of Thin Films

J. Phys. Chem. B, Vol. 108, No. 51, 2004 **19771**

system preferentially occupies at a given temperature, and it also is the value of ϕ that minimizes the right-hand side of eq 3 under conditions of fixed β, ρ, and L. The quantity $-\sigma(\phi^*,\rho,L)/\beta = -Ts_C$ represents the contribution to the free energy associated with the number of basins accessible to the equilibrium film, and thus s_C is typically referred to as the *configurational entropy*. At elevated temperatures, one expects higher values of ϕ^* and s_C to be obtained because thermal energy can carry the system over potential energy barriers, giving it access to a substantial fraction of the higher lying basins. On the other hand, if the temperature of the film is lowered, ϕ^* and s_C will decrease because the system will be driven down the energy landscape, where it is constrained to a smaller subset of deeper basins. One can imagine the possibility that, if the film were cooled to sufficiently low temperature without crystallizing, the configuration point could become trapped in the single deepest amorphous basin on the landscape, forming the so-called *ideal glass* (IG) state (see Figure 2).[19,20]

These two potential states for amorphous condensed-phase films, an equilibrium fluid at high temperature and an ideal glass at low temperature, correspond to two simple and distinct mathematical conditions for ϕ^*:

$$\left[\left(\frac{\partial\sigma}{\partial\phi}\right)_{\beta,\rho,L}\right]_{\phi=\phi^*} = \left[\beta\left\{1 + \left(\frac{\partial f_{vib}}{\partial\phi}\right)_{\beta,\rho,L}\right\}\right]_{\phi=\phi^*} \qquad \beta < \beta^{IG}(\rho,L) \tag{4}$$

and

$$\phi^* = \phi_{min}(\rho,L) \qquad \beta \geq \beta^{IG}(\rho,L) \tag{5}$$

where $\beta^{IG}(\rho,L)$ denotes the reciprocal ideal glass transition temperature. Of course, eq 5 does not imply the existence of an ideal glass transition for any real or model material at finite temperature; rather, it provides a landscape-based thermodynamic framework for addressing the possibility. In section III, we explore the predictions of a specific model film that exhibits an ideal glass transition.

Landscape-Based Equation of State. The development presented above illustrates how the equilibrium free energy of a thin film is formally connected to the manner in which its configuration point $\mathbf{r}^N$ explores the potential energy landscape. Here, we use classical thermodynamics to derive the associated landscape-based expression for the film's equation of state. The appropriate thermodynamic potential to consider in this case is the Helmholtz free energy per particle f, and its differential for fixed N is given by[21]

$$df = \left(\frac{s}{k_B\beta}\right)\frac{d\beta}{\beta} + \left(\frac{p^{||}}{\rho}\right)\frac{d\rho}{\rho} + \left(\frac{p^{||} - p^{\perp}}{\rho}\right)\frac{dL}{L} \tag{6}$$

where s is the molar entropy and $p^{||}$ and $p^{\perp}$ are the diagonal components of the pressure tensor associated with directions transverse and normal to the confining substrates, respectively:

$$p^{||} = \rho^2\left(\frac{\partial f}{\partial\rho}\right)_{\beta,L}$$

$$p^{\perp} = p^{||} - \rho L\left(\frac{\partial f}{\partial L}\right)_{\beta,\rho} \tag{7}$$

Differentiating f of eq 3 as prescribed by eq 7 leads to the

following relationships, which are valid for films in either the fluid or the ideal glass state:

$$p^{||} = p^{||}_{IS} + p^{||}_{vib}$$

$$p^{||}_{IS} = \rho^2\left(\frac{\partial\phi^*}{\partial\rho}\right)_{\sigma,\beta,L}$$

$$p^{||}_{vib} = \rho^2\left[\left(\frac{\partial f_{vib}}{\partial\phi}\right)_{\beta,\rho,L}\left(\frac{\partial\phi^*}{\partial\rho}\right)_{\sigma,\beta,L} + \left(\frac{\partial f_{vib}}{\partial\rho}\right)_{\phi,\beta,L}\right]_{\phi=\phi^*} \tag{8}$$

and

$$p^{\perp} = p^{\perp}_{IS} + p^{\perp}_{vib}$$

$$p^{\perp}_{IS} = p^{||}_{IS} - \rho L\left(\frac{\partial\phi^*}{\partial L}\right)_{\sigma,\beta,\rho}$$

$$p^{\perp}_{vib} = p^{||}_{vib} - \rho L\left[\left(\frac{\partial f_{vib}}{\partial\phi}\right)_{\beta,\rho,L}\left(\frac{\partial\phi^*}{\partial L}\right)_{\sigma,\beta,\rho} + \left(\frac{\partial f_{vib}}{\partial L}\right)_{\phi,\beta,\rho}\right]_{\phi=\phi^*} \tag{9}$$

This separation of inherent structure (IS) and vibrational (vib) contributions to the pressure tensor follows directly from a recent theory for the out-of-equilibrium free energy of bulk glass-forming materials.[22,23] As can be seen from eqs 8 and 9, $p^{||}_{IS}$ and $p^{\perp}_{IS}$ characterize how density and film thickness affect the topograpy of the energy landscape and, consequently, the depth of the basins that are thermodynamically accessible to the system's configuration point. Specifically, $p^{||}_{IS}$ characterizes how ϕ^* varies with density along a path of constant film thickness, temperature, and configurational entropy. Similarly, $(p^{||}_{IS} - p^{\perp}_{IS})$ quantifies how ϕ^* varies with film thickness along a path of constant density, temperature, and configurational entropy. Of course, $p^{||}_{IS}$ and $p^{\perp}_{IS}$ also have a mechanical interpretation: they represent the ensemble-averaged virial components of the pressure tensor for inherent structures sampled by the equilibrium film at β, ρ, and L. The vibrational contributions, $p^{||}_{vib}$ and $p^{\perp}_{vib}$, account for the balance of the pressure tensor, and they reflect how changes in density and film thickness affect intrabasin thermal excitations of the configuration point.

Systematic investigations of the inherent structure contribution to the equation of state for bulk homogeneous materials have been carried out by computer simulation.[24−28] These studies have shown that there is generally a characteristic relationship between the average isotropic pressure (or tension) of inherent structures p_{IS} and density ρ: the so-called "equation of state of an energy landscape" shown schematically in Figure 3.[25] This relationship appears to be only weakly dependent on temperature for simple liquids above their freezing point.[14,25,29] The following trends have also been generally noted. Inherent structures formed with densities higher than the material's Sastry density ρ_S are structurally homogeneous, whereas those formed at densities lower than ρ_S contain large cracks or voids.[25] In other words, ρ_S appears to be the minimum density for which an amorphous material can simultaneously maintain mechanical stability and structural homogeneity. This suggests that ρ_S is a bulk material property that represents the low-density limit for homogeneous glass formation. As is shown in Figure 3, the isotropic tension obtained at the Sastry density $p_{IS}(\rho_S)$ represents the maximum amount that a homogeneous sample of that material can sustain prior to fracture.
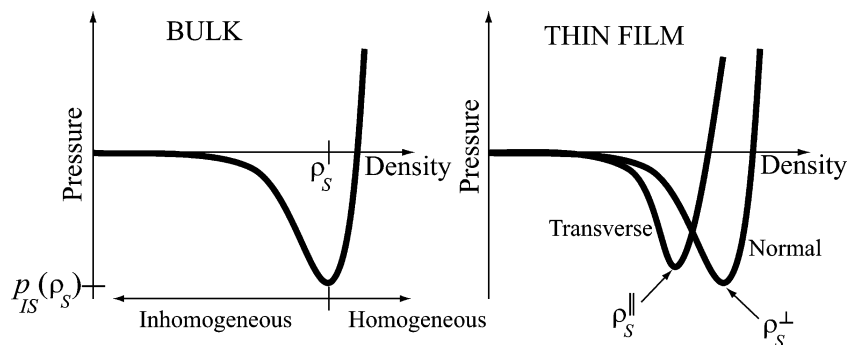
Figure 3. Qualitative form of inherent structure pressure as a function of density in bulk isotropic (left) and thin film (right) materials. The minimum in the left-hand curve corresponds to the Sastry density[25] ρ_S discussed in the text. Thin-film materials exhibit two components of the pressure tensor (normal and transverse) and two associated Sastry densities $\rho_S^\perp$ and $\rho_S^\parallel$.

This type of inherent structure analysis has not yet been performed on model thin films. However, one expects films to exhibit richer behavior than bulk materials because interfacial interactions render them anisotropic and statistically inhomogeneous, even in the fluid and glassy states. As a result, films will exhibit two distinct versions of the curve shown in Figure 3, representing the dependencies of $p_{IS}^\parallel$ and $p_{IS}^\perp$ on density. In analogy to bulk materials, one expects that there will also be a critical film density ρ_S below which inherent structures will "fail" by forming large cracks or voids (i.e., a Sastry density for films). However, it is not clear at the outset whether this density will correspond to the maximum normal tension or the maximum transverse tension that the film can sustain. In other words, it is not obvious in which direction the film will be more vulnerable to mechanical failure. Nor is it obvious how the dimensions of the film or the film and substrate interactions will impact this vulnerability. Of course, a complete understanding of these issues will require extensive investigation by experiments, simulation, and theory. In this Article, we take a first step in that direction by introducing a general theoretical framework and a simple mean-field model for calculating inherent structure and vibrational contributions to the pressure tensor of thin films.

Model Thin Film. The model material that we consider for our film is the soft-sphere/mean-field (SSMF) fluid. It has served as the focus of several recent theoretical investigations (albeit, in bulk homogeneous conditions) because (i) its thermodynamic properties qualitatively reproduce the experimentally observed trends for simple liquids, and (ii) its potential energy landscape exhibits scaling properties that make it particularly convenient to analyze.[14,15,23] The SSMF model is so named because its N structureless particles interact via soft-sphere repulsions $\epsilon(\sigma_{SS}/r)^n$ balanced by a uniform mean-field attraction of the form $-Na_b\rho$. The parameters ϵ and σ_{SS} set the characteristic energy and length scales of the soft-sphere repulsion, n determines its "steepness", and a_b quantifies the cohesive energy associated with attractive interactions between the particles. To simplify the notation in our analysis, we take all thermodynamic variables and model parameters to be implicitly nondimensionalized by appropriate combinations of ϵ and σ_{SS}.

Under bulk homogeneous conditions, the potential energy per particle of the SSMF fluid $\varphi(\mathbf{s}^N,\rho)$ can be expressed in terms of the scaled coordinates of the particles $\mathbf{s}_i$ ($i = 1, ..., N$) as[30]

$$\varphi(\mathbf{s}^N,\rho) = -a_b\rho + y(\mathbf{s}^N)\,\eta(\rho)^{n/3} \qquad (10)$$

where $\eta(\rho) = \pi\rho/6$ is the effective packing fraction of the

molecules, and $y(\mathbf{s}^N)$ is a density-independent function formally defined as

$$y(\mathbf{s}^N) \equiv N^{-1}(6/\pi N)^{n/3}\sum_{i=1}^{N-1}\sum_{j=i+1}^{N} s_{ij}^{-n} \qquad (11)$$

with $s_{ij} = |\mathbf{s}_i - \mathbf{s}_j| = V^{-1/3}|\mathbf{r}_i - \mathbf{r}_j|$ representing the dimensionless interparticle separation. We consider the situation where two parallel "hard wall" substrates (each with surface area A) physically confine the SSMF particle centers to a film of volume $V = AL$ (see Figure 1) and interact with them through a mean-field attraction. In this case, the packing fraction η, the van der Waals attraction parameter a, and the soft-sphere energy function y will generally depend on film thickness L, and thus φ can be expressed

$$\varphi(\mathbf{s}^N,L,\rho) = -a(L)\rho - \Psi(L) + y(\mathbf{s}^N, L)\,\eta(\rho,L)^{n/3} \quad (12)$$

where $-\Psi(L)$ denotes the uniform attractive interaction between the film particles and the confining substrates. Mean-field relations for $a(L)$, $\Psi(L)$, and $\eta(\rho,L)$ (see Appendix A) are given by[31,32]

$$a(L) = a_b\left[1 - \frac{3}{4L} + \frac{1}{8L^3}\right] \qquad 1 \leq L < \infty$$

$$= a_b\left[\frac{3L}{8}\right] \qquad 0 < L < 1 \qquad (13)$$

$$\eta(\rho,L) = \frac{\pi\rho}{6}\left[1 - \frac{3}{16L}\right] \qquad {}^1\!/_2 \leq L < \infty$$

$$= \frac{\pi\rho}{6}\left[\frac{3L}{2} - L^3\right] \qquad 0 < L < {}^1\!/_2 \qquad (14)$$

$$\Psi(L) = \Psi_0\left[\frac{1}{L} - \frac{1}{L(1 + L)^2}\right] \qquad 0 < L < \infty \qquad (15)$$

The parameter Ψ_0 in eq 15 provides the coarse energy scale for the film–substrate attractions, and its connection to the details of the film–substrate intermolecular pair potential has been discussed previously.[31,32] As a first approximation, we will assume that $y(\mathbf{s}^N,L) \simeq y(\mathbf{s}^N)$, i.e., that the dependence of the total soft-sphere energy on film thickness comes only from the L-dependent packing fraction $\eta(\rho,L)$. This assumption should provide a reasonably accurate description of thicker (nearly homogeneous) films, but it cannot be expected to hold for ultrathin films that are highly inhomogeneous.

To develop a tractable landscape-based analytical theory for the SSMF film, we make three additional simplifications that

Predicting the Properties of Thin Films

J. Phys. Chem. B, Vol. 108, No. 51, 2004 **19773**

we outline below. These assumptions are commonly invoked (see, e.g., ref 23) to analyze the energy landscapes of bulk materials; however, they remain approximations even within the context of a given model. Thus, they should be viewed as imperfect, but workable, starting points for analytical theories of thin films that, once again, should be verified when possible by comparison to experiments and "exact" simulations.

First, we take the vibrational contribution to the Helmholtz free energy to be independent of basin depth, i.e., $\partial f_{vib}/\partial \phi = 0$. This assumption becomes exact in the $\beta \rightarrow \infty$ limit, where both f_{vib} and $\partial f_{vib}/\partial \phi$ vanish by definition. For finite temperature, this approximation amounts to assuming that "basins of the same depth have the same shape". This assumption has been applied in several landscape-based theories,[23] in part because it greatly simplifies the analysis (e.g., here it simplifies eqs 4, 8, and 9). However, one should keep in mind that realistic systems generally exhibit a distribution of basin shapes at a given elevation on the landscape.

Next, we assume that we can treat the vibrational contribution to the Helmholtz free energy in the classical harmonic approximation, $f_{vib} = 3\beta^{-1} \ln[\beta k_B \Theta_E]$, where Θ_E is the Einstein temperature of the film. Given the interactions of our model and the assumption that $\partial f_{vib}/\partial \phi = 0$, this implies the following form for f_{vib} (see, e.g., refs 23 and 33):

$$f_{vib} = 3\beta^{-1} \ln[c_0 \beta \eta(\rho,L)^{(n+2)/6}] \quad (16)$$

Here, c_0 is a constant that depends on the mass of the particles but not on temperature or density. As a result, c_0 cannot affect the film's phase behavior, the ideal glass transition, the equation of state, or the properties of its inherent structures. Because these are the primary quantities of interest in the present study, we can set $c_0 = 1$ without loss of generality. In "cold" condensed phases, eq 16 should be reasonably accurate, but one expects this expression to be less reliable at high temperatures where anharmonic excitations become important.

Finally, we assume that the energy landscape exhibits a Gaussian distribution of basin depths. Specifically, we take the basin enumeration function $\sigma(\phi,\rho,L)$ to have the following form:

$$\frac{\sigma(\phi,\rho,L)}{\sigma_\infty} = 1 - \left[\frac{\phi - \phi_\infty(\rho,L)}{\phi_\infty(\rho,L) - \phi_{min}(\rho,L)}\right]^2$$
$$\phi_{min}(\rho,L) < \phi < \phi_\infty(\rho,L) \quad (17)$$

This relationship, when considered along with eq 4 and the assumption that $\partial f_{vib}/\partial \phi = 0$, implies that the film will sample basins of depth $\phi_\infty(\rho,L)$ in the infinite temperature limit and that it can become trapped in the deepest basin $\phi_{min}(\rho,L)$ at finite temperature, forming an ideal glass. Although there are other possible functional forms for σ, the Gaussian distribution of basin depths given by eq 17 is one of the simplest and most commonly applied approximations for the energy landscapes of bulk materials.[23,34]

Using the above-described assumptions along with eqs 4, 5, and 12−17, we can derive the following expressions for the reciprocal ideal glass transition temperature β^{IG},[35]

$$\beta^{IG} = \frac{2\sigma_\infty}{[y_\infty - y_{min}]\eta(\rho,L)^{n/3}} \quad (18)$$

the inherent structure energy ϕ^*

$$\phi^* = y_\infty \eta(\rho,L)^{n/3} - \frac{(y_\infty - y_{min})^2}{2\sigma_\infty}\beta\eta(\rho,L)^{2n/3} -$$
$$a(L)\rho - \Psi(L) \quad \beta < \beta^{IG}(\rho,L)$$
$$= y_{min}\eta(\rho,L)^{n/3} - a(L)\rho - \Psi(L) \quad \beta \geq \beta^{IG}(\rho,L) \quad (19)$$

and the configurational entropy $s_C = k_B \sigma(\phi^*,\rho,L)$

$$s_C = k_B \sigma_\infty \left\{1 - \left[\frac{(y_\infty - y_{min})}{2\sigma_\infty}\beta\eta(\rho,L)^{n/3}\right]^2\right\} \quad \beta < \beta^{IG}(\rho,L)$$
$$= 0 \quad \beta \geq \beta^{IG}(\rho,L) \quad (20)$$

In the above, y_{min} and y_∞ represent $y(\mathbf{s}^N)$ of eq 11 evaluated at ϕ_{min} and ϕ_∞, respectively. The Helmholtz free energy of the film can then be obtained by combining eq 3, 17, and 19 to get

$$f = y_\infty \eta(\rho,L)^{n/3} - \frac{\sigma_\infty}{\beta}\left\{1 + \left[\frac{(y_\infty - y_{min})}{2\sigma_\infty}\beta\eta(\rho,L)^{n/3}\right]^2\right\} -$$
$$a(L)\rho - \Psi(L) + \frac{3}{\beta}\ln[\beta\eta(\rho,L)^{(n+2)/6}] \quad \beta < \beta^{IG}(\rho,L)$$
$$= y_{min}\eta(\rho,L)^{n/3} - a(L)\rho - \Psi(L) + \frac{3}{\beta}\ln[\beta\eta(\rho,L)^{(n+2)/6}]$$
$$\beta \geq \beta^{IG}(\rho,L) \quad (21)$$

Other thermodynamic properties of the SSMF film, e.g., the transverse and normal components of the pressure tensor and the chemical potential $\mu = f + p^\parallel \rho^{-1}$, follow from eqs 7 and 21.

To perform calculations with the model, we must specify numerical values for the parameters n, σ_∞, y_∞, y_{min}, a_b, and Ψ_0. For this study, we use $n = 12$, $\sigma_\infty = 0.5368$, $y_\infty = 61.73$, $y_{min} = 53.22$, and $a_b = 16.5$. This set of parameters was chosen because it provides good qualitative agreement with both the liquid-state thermodynamics and the predicted IG transition locus of the bulk Lennard-Jones system.[23,36] In section III, we explore how the magnitude of the fluid−substrate attraction parameter Ψ_0 and the film thickness L affect the ideal glass transition temperature, the mechanical properties of the inherent structures, and the phase diagram of the thin film.

III. Results

Shift of the Ideal Glass Transition. Here, we use the mean-field theory of section II to predict how film thickness L and strength of the fluid−substrate attractions Ψ_0 modify the IG transition temperature $T^{IG} = (k_B \beta^{IG})^{-1}$. As is discussed elsewhere,[35] there are two complementary approaches for studying this issue. The first is a method that involves performing a first-order perturbation expansion of the SSMF film equations in powers of reciprocal film thickness. This approach is strictly valid only in the "thick film" limit, but it produces analytical relationships that give new physical insights into the effects of confinement on the IG transition. A second approach is to solve the full nonlinear SSMF film model for T^{IG} numerically. This approach is valid for films of arbitrary thickness, and so it provides a stringent test for the accuracy of the analytical perturbation equations. More details about the calculation of the IG transition temperature of the film are given in Appendix B.

The perturbation approach provides three equivalent analytical expressions for $\Delta T^{IG}/T_b^{IG}$ valid to first order in L^{-1}, which we

review below. The first expression conveys the "topographical" view of the IG transition and is given by[35]

$$\frac{\Delta T^{IG}}{T_b^{IG}} = -\frac{1}{\Delta c_P^{IG}(p_b)}\left[\left\{\frac{\partial s_C(1/L, p_b, T^{IG})}{\partial(1/L)}\right\}_{p_b}\right]_{L\to\infty}\left(\frac{1}{L}\right) \quad (22)$$

where $\Delta c_P^{IG}(p_b) = (\partial s_C/\partial \ln T)_{p_b}$ is the configurational heat capacity of the bulk fluid at its IG transition. Equation 22 has a simple interpretation: it relates the shift in the IG transition temperature of the film to the confinement-induced change in its configurational entropy relative to the bulk. Because $\Delta c_P^{IG}(p_b) > 0$, one can see that T^{IG} is depressed if confinement increases the number of basins accessible to the film (hence, increasing s_C). Conversely, if confinement reduces the number of accessible basins, then the IG transition temperature is raised. This is a general relationship between film thickness, configurational entropy, and the IG transition temperature in the energy landscape framework.

The second analytical relation provided by the perturbation approach[35] connects the shift in the IG transition to thermodynamic properties of the film:

$$\frac{\Delta T^{IG}}{T_b^{IG}} = \frac{1}{\kappa_T^{IG}(p_b)}\left(\frac{2\Gamma_b^{IG}(p_b)}{\rho_b^{IG}(p_b)} - \frac{3}{16}\right)\left[\frac{\mathrm{d}\ln T_b^{IG}(p_b)}{\mathrm{d}p_b}\right]\left(\frac{1}{L}\right) \quad (23)$$

Here, $2\Gamma_b^{IG}(p_b) = [\rho^{IG}(L, p_b) - \rho_b(p_b, T^{IG})]L$ is the surface excess density and $\kappa_T^{IG}(p_b) = (\partial \ln \rho/\partial \ln p_b)_{T_b^{IG}}$ is the isothermal compressibility, each evaluated at the IG transition of the fluid film in the bulk limit, i.e., $[L\to\infty, p_b, T_b^{IG}(p_b)]$. Because T_b^{IG} increases monotonically with p_b in this model, the IG transition shift is controlled by the magnitude and sign of the surface excess density. Small or negative values of the surface excess density mean that physical confinement results in a film T^{IG} that is lower than the bulk, whereas large positive values of the surface excess density should have the opposite effect. Restated simply, if a thin film is less dense than the bulk fluid, then its T^{IG} will be reduced; whereas if a film is denser than the bulk phase, its T^{IG} will be higher. This is consistent with McCoy and Curro's recently proposed "density-based" theory for the confinement-induced shift in the glass transition temperature.[37]

The third equality provided by the perturbation approach establishes a connection to molecular parameters of the SSMF film model:[35]

$$\frac{\Delta T^{IG}}{T_b^{IG}} = \left(\Psi_0 - \frac{9a_b\rho_b^{IG}(p_b)}{8}\right)\rho_b^{IG}\left[\frac{\mathrm{d}\ln T_b^{IG}(p_b)}{\mathrm{d}p_b}\right]\left(\frac{1}{L}\right) \quad (24)$$

and it also conveys a simple physical picture. Strongly attractive walls relative to the cohesive energy of the film $\Psi_0/a_b \gg 1$ tend to elevate the IG transition temperature, whereas neutral or repulsive walls $\Psi_0/a_b \approx 0$ tend to depress T^{IG}. This prediction is in good qualitative agreement with the trends for the kinetic glass transition observed in experiments and computer simulations of confined fluids and thin films (see, e.g., refs 2–6, 9, and 37).

Figure 4 shows the confinement-induced shifts in the IG transition temperature as predicted by the perturbation theory (i.e., eq 22, 23, or 24) and the full nonlinear SSMF film model given in section II. As can be seen, the shift of the IG transition is approximately inversely proportional to film thickness, indicating that the perturbation theory provides a very accurate representation of the full nonlinear model down to molecular-scale films. This, in fact, should cover the range of film thickness
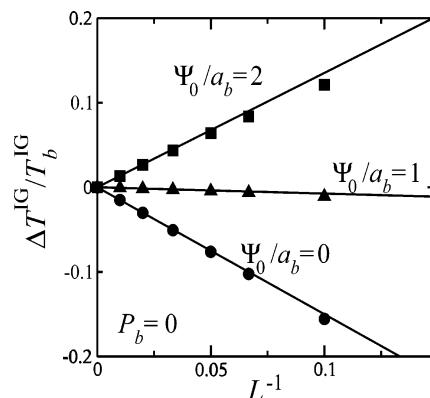

Figure 4. Confinement induced shift in the IG transition of the SSMF film relative to that of the bulk system with which it is in equilibrium at pressure $p_b = 0$. L^{-1} is the dimensionless reciprocal film thickness accessible to the film particle centers. The solid lines represent the approximation of eq 22, and the symbols are the predictions of the full nonlinear model of section II. The relative strength of the film–substrate to cohesive film attractions is quantified by $\Psi_0/a_b = 2$ (strongly attractive substrates), $\Psi_0/a_b = 1$ (neutral substrates), and $\Psi_0/a_b = 0$ (hard walls).

where one expects the most reliable predictions from the SSMF film model, because the uniform density profile assumption (see eq 12) is known to break down in the limit of very thin films, where density profiles are highly inhomogeneous.

Mechanical Properties of Thin-Film Inherent Structures. As discussed in section II, the anisotropic nature of the pressure tensor for thin-film inherent structures should give rise to an "equation of state of an energy landscape" ($p_{IS}^\perp$ and $p_{IS}^{\parallel}$ versus ρ) that is richer than the scalar version exhibited by isotropic materials (p_{IS} versus ρ). To understand why, consider the following questions that naturally arise for a given thin film. First, which component of the pressure tensor will display a "Sastry minimum" at a higher density (i.e., a lower transverse strain)? In other words, upon a decrease in the film density at constant L from high to low values (see Figure 3), will the normal or transverse Sastry density (i.e., $\rho_S^\perp$ or $\rho_S^{\parallel}$) be encountered first? What will be the physical consequences? Will mechanical failure and the formation of structural voids occur simultaneously at that point, as is observed[25–28,14,15] in isotropic inherent structures? Moreover, will $\rho_S^\perp$ and $\rho_S^{\parallel}$ correspond to fundamentally distinct types of failure modes (e.g., adhesive failure versus cavitation[38])? Finally, how will the answers to these questions depend on film thickness and strength of the film–substrate and film-film attractions?

Many of these issues cannot be addressed with an analytical mean-field theory, and thus they should be further investigated by molecular simulation and experiments. However, to help organize our thoughts, we can use the landscape-based SSMF film theory of section II to provide some initial predictions. In particular, we can study the following question. If we fix both the film thickness L and the ratio of the fluid–substrate attraction parameter Ψ_0 to the film cohesive energy parameter a_b, which type of Sastry density will be larger, $\rho_S^\perp$ or $\rho_S^{\parallel}$? If, as appears to be the case for isotropic materials,[25–28,14,15] these respective Sastry densities correspond to limits of mechanical stability for inherent structures, then the answer to the above question will provide new insights into how the physical properties of thin films affect their vulnerability to failure in the normal and transverse directions.

To make this point concrete, consider Figure 5, which shows the locus of points satisfying $\rho_S^\perp = \rho_S^{\parallel}$ in the $(\Psi_0/a_b) - L^{-1}$ plane as predicted by the SSMF film theory. Similar to the cases
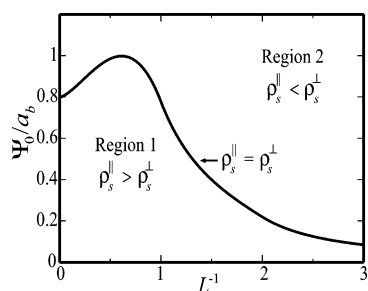
Predicting the Properties of Thin Films

J. Phys. Chem. B, Vol. 108, No. 51, 2004 **19775**

Figure 5. Parameter space of film−substrate to cohesive film attractions Ψ_0/a_b versus degree of confinement L^{-1} for the inherent structures of the SSMF film model. The solid curve maps the locus of film parameters for which the condition $\rho_S^{\parallel} = \rho_S^{\perp}$ is satisfied by the inherent structures. Possible implications for mechanical stability and failure of thin films are discussed in the text.

considered in simulations of isotropic materials,[25−28,14,15] we consider inherent structures quenched from high temperatures (here, strictly $\beta \rightarrow 0$). The analytical expressions that determine the conditions for the above equality are presented in Appendix C. The plot shows two distinct regions of parameter space for thin films, illustrating the combined effects that substrate attractions and confinement have on the mechanical properties of thin-film inherent structures. Region 1 corresponds to films with $\rho_S^{\parallel} > \rho_S^{\perp}$ and region 2 corresponds to films with $\rho_S^{\parallel} < \rho_S^{\perp}$. In other words, high-density films in region 1 would first arrive at $\rho_S^{\parallel}$ upon transverse expansion at constant L, whereas high-density films in region 2 would first encounter $\rho_S^{\perp}$. If $\rho_S^{\parallel}$ and $\rho_S^{\perp}$ actually correspond to limits of mechanical stability, as ρ_S does for isotropic inherent structures, then one can think of Figure 5 as a *failure vulnerability diagram*, with films in regions 1 and 2 being more susceptible to failure in the transverse and normal directions, respectively.

Although there are caveats to consider when interpreting Figure 5, we want to first focus on understanding the predictions of the model. Specifically, we want to explore what physical factors control the values of $\rho_S^{\parallel}$ and $\rho_S^{\perp}$. An analysis of the contributing terms provided in Appendix C provides the following qualitative picture. The values of $\rho_S^{\parallel}$ and $\rho_S^{\perp}$ (i.e., the minima in the $p_{IS}^{\parallel}$ and $p_{IS}^{\perp}$ versus ρ) are determined by a balance between stress contributions from interparticle repulsions (due to packing forces), attractions between particles in the film (proportional to a_b), and attractions between the film and the substrate (proportional to Ψ_0). First, consider thick films with $L^{-1} \ll 1$. All other factors being equal, any relative increase in the mechanical stresses due to attractive forces in a particular direction, transverse or normal, will preferentially result in a higher value of the Sastry density for that direction. For example, if the substrates do not experience attractions with the film ($\Psi_0/a_b = 0$), then, for simple geometric reasons, the attractions between the molecules in the film will exert a comparatively larger cohesive stress in the transverse direction, and the result will be $\rho_S^{\parallel} > \rho_S^{\perp}$. Conversely, making the substrates more attractive by increasing the ratio Ψ_0/a_b can compensate for the reduction of normal cohesive forces and ultimately lead to a comparatively higher *net* attractive stress in the normal direction, resulting in $\rho_S^{\parallel} < \rho_S^{\perp}$. If the films become thinner (larger L^{-1}), larger substrate attractions are required to compensate for the lost film cohesive stresses in the normal direction, resulting in the initially positive slope of the $\rho_S^{\perp} = \rho_S^{\parallel}$ curve in Figure 5.

For very thin films, the model predicts that packing effects also become important. In particular, it predicts that packing forces result in a comparatively higher repulsive contribution

to the stress in the transverse direction, which mediates the corresponding cohesive attractive stress. As a result, smaller film−substrate attractions are required to cause the transition from $\rho_S^{\parallel} > \rho_S^{\perp}$ to $\rho_S^{\parallel} < \rho_S^{\perp}$ scenarios. This is the cause for the negatively sloped $\rho_S^{\parallel} = \rho_S^{\perp}$ curve for large L^{-1} in Figure 5. However, we should emphasize an important point concerning the aforementioned packing effects in our model. They occur at film thicknesses that are far below where the mean-field assumptions of the SSMF film model should break down. In fact, because the SSMF film model ignores the details of the density profiles characteristic of very thin films, it may also be missing out on important physics that dominate vulnerability to failure. Namely, the layering effects of molecules in thin films might provide natural "weak spots" parallel to the substrate that lead to mechanical failure in the normal direction. This issue deserves further investigation with molecular simulations and, perhaps, a density-functional version of the present landscape-based theory.

We further note two model-independent caveats that naturally arise in interpreting Figure 5 as a failure vulnerability diagram. First, despite the appealing analogy with inherent structures of bulk isotropic systems, there is no current evidence that thin-film inherent structures mechanically fail or form voids at $\rho_S^{\parallel}$ or $\rho_S^{\perp}$. We are currently examining this intriguing question via molecular simulation, and the results of that study will be the subject of a future publication. Second, the failure modes of thin-film inherent structures are not necessarily the same as (or connected to) the failure modes of the same thin films at finite temperature, where vibrational contributions and nonequilibrium effects could play an important role. One useful data point in understanding this issue is the recent molecular simulation study of adhesive failure in polymeric thin films of Gersappe and Robbins,[39] which suggests that enthalpy is more important than entropy in determining the actual mechanism for mechanical failure. However, the generality of this conclusion is largely unknown, and it remains an intriguing area for future inquiry.

Thin-Film Thermodynamics. Confinement fundamentally changes the character of the thermodynamics of a material. The equilibrium scalar pressure becomes a tensor (as discussed in the previous section), the "bulk" coexistence curves on the phase diagram are generally modified in a manner that depends on both sample size and the physical properties of the bounding interfaces, and the possibility arises for new surface-induced thermodynamic phases that are dictated by the geometry and the microscopic interactions of the sample and the confining medium. Moreover, because the stable equilibrium states of nano-confined materials play a key role in determining their structural, mechanical, electrical, and optical properties, there is considerable interest in developing fundamental tools that can predict the general effects of confinement on the phase diagram.

The SSMF film model presented here allows for the systematic investigation of the equilibrium thermodynamics as a function of film thickness L and strength of the film−substrate attractions Ψ_0. However, because it assumes at the outset that the film displays a uniform density throughout its interior, this approach will not be able to provide insight into layering, prewetting, or buckling transitions,[1] where the relevant order parameters depend on the inhomogeneous structural properties of the participating phases. This is a shortcoming of the theory— one that can ultimately be improved upon in the future by introducing a density-functional version of the landscape-based approach. Nonetheless, even the simple coarse-grained model presented here is able to predict many of the general effects of
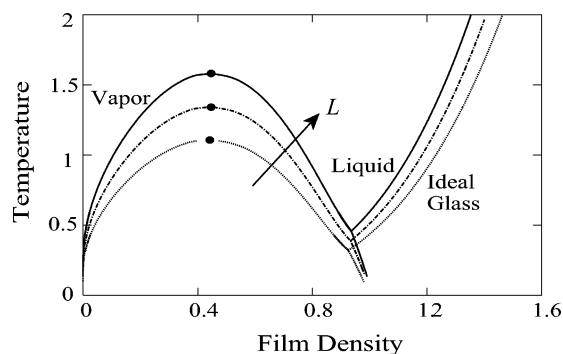
Figure 6. Phase diagrams for the SSMF bulk (solid curve) and the SSMF film model for $L = 5$ (dot−dashed) and $L = 2.5$ (dotted) in the temperature T versus film density ρ plane.

confinement on both the vapor−liquid phase boundary and the ideal glass transition locus. We explore some of those predictions below.

Figure 6 shows projections of the equilibrium phase diagrams of the SSMF bulk system and films of thickness $L = 5$ and 2.5 in the temperature T versus film density ρ plane. Recall that L is given in units of particle diameters, and it represents the dimension of the film that is normal to the substrates and accessible to the particle centers (see Figure 1). The loci of phase coexistence in Figure 6 were calculated by requiring film phases to simultaneously maintain equality of transverse pressure $p^{\parallel}$ and chemical potential $\mu = f + p^{\parallel}\rho^{-1}$, quantities that are readily calculated from eqs 7 and 21 (see also Appendix C). The general thermodynamic considerations of confined films such as those analyzed here have been studied extensively, and the main issues are summarized elsewhere.[1,21,40]

The IG transition loci of the SSMF films were calculated from eq 18. Note that there is a single curve (for each system) in the $T-\rho$ plane of Figure 6 corresponding to the IG transition locus. This simply reflects the fact that the IG transition is a second-order equilibrium phase transition in the Gaussian landscape approximation of eq 17 (see also, e.g., ref 23), and thus there can be no change in density when the liquid-state vitrifies to form the ideal glass.

Another notable feature of Figure 6 is that the thin films exhibit a downward shifted version of the "bulk" liquid−vapor phase transition (referred to as the capillary condensation transition for confined fluids). This downward shift is in good qualitative agreement with the trends observed in experiments, simulations, and theories of fluids confined to slit-pore geometries.[1,40] At very low temperatures, the vapor−liquid phase boundary is predicted to intersect the ideal glass transition, forming a vapor−liquid−ideal glass triple point, a scenario discussed earlier by Sastry.[41] For temperatures below this triple point, there is no longer a stable vapor−liquid transition but, instead, only a vapor-ideal glass equilibrium.

Finally, we point out that the $T-\rho$ projections of the phase diagrams of Figure 6 are predicted by the SSMF film model to be independent of the strength of fluid-substrate attractions Ψ_0. This prediction follows from the fact that the transverse component of the pressure tensor in the SSMF film model (see Appendix C) is independent of Ψ_0. However, it is important to emphasize here that Ψ_0 will have an effect on the phase behavior even in the framework of the SSMF film model, *if the film is required to remain in thermodynamic equilibrium with a bulk phase*. This connection stems from the equilibrium requirement of equal chemical potentials between the film (where μ depends on Ψ_0) and the bulk (where μ is independent of Ψ_0). Schoen and Diestler have addressed this issue in detail in a previous

publication.[31] One obvious manifestation of the effect of substrate attractions on the state of the SSMF film is the shift in the ideal glass transition temperature that was discussed at length at the beginning of the Results. Another well-known effect of substrate attractions that can be reproduced by the present model (but not shown here) is the fact that the bulk pressure required for capillary condensation of fluids in porous materials depends sensitively on the strength of the attractions between the fluid and the pore (see, e.g., ref 42).

IV. Conclusions

In this Article, we develop an analytical energy landscape based mean-field theory for studying the physical behavior of thin films confined between parallel substrates. We use the theory to explore how the dimensions of thin films and their interactions with substrates can influence both the equilibrium phase diagram and the ideal glass transition locus. The predictions are encouraging because they are in good general agreement with many of the experimentally observed trends for confined fluids and thin films. They also provide compelling evidence that the energy landscape is viable as a general tool for studying how nanoscale confinement affects the thermodynamic and kinetic properties of materials.

A second, thought-provoking result of the landscape based theory is that it yields an analytical expression for the average pressure tensor of thin-film inherent structures as a function of film density, film thickness, and the strength of fluid-substrate attractions (see Appendix C). This is, to our knowledge, the first theoretical prediction of an "equation of state of an energy landscape" for thin films. The tensorial nature of the pressure in anisotropic systems changes the character of this relationship as compared to the scalar version that has been measured and analyzed in simulations of isotropic materials. In particular, both the normal and the transverse components of the pressure tensor of thin-film inherent structures exhibit distinct minima with respect to film density; i.e., there are two Sastry densities. If the analogy to the behavior of isotropic inherent structures holds, one expects that these points of maximum tensile strength in the normal and transverse directions are related to limits of mechanical stability. The theory presented here allows us to predict how film dimensions and film−substrate attractions control which of the two pressure component minima (transverse or normal) occurs at a higher density. We use these predictions to construct a failure vulnerability diagram that suggests how the properties of thin films impact their susceptibility to different types of mechanical failure. We are currently following up on our theoretical predictions with an extensive investigation of the mechanical properties of thin-film inherent structures via molecular simulation.

Despite these successful predictions, the present level of the theory is still not detailed enough to address some of the outstanding issues concerning the structural, mechanical, and thermodynamic behavior of thin films. In this sense, the development of landscape based approaches for confined materials is still in its infancy. However, because computer simulations can be used to provide an essentially exact picture for how material systems sample their energy landscapes, there is tremendous opportunity for testing and systematically improving upon the approximations that are currently being employed. One area that deserves particular attention is the assumption of a uniform density. Real confined materials exhibit strongly inhomogeneous density profiles. There is no doubt that these profiles impact the thermodynamics (producing layering and prewetting transitions), the kinetics (causing spatially

Predicting the Properties of Thin Films

J. Phys. Chem. B, Vol. 108, No. 51, 2004 **19777**

inhomogeneous dynamics), and mechanical properties (perhaps providing "weak spots" for failure). To begin to address these issues, we are currently developing a density functional version of the landscape based theory for thin films, which we will outline in future publication.

Appendix A: Mean-Field Parameters for the SSMF Film

A derivation for the film−substrate mean-field attraction parameter $\Psi_0(L)$ valid for arbitrary film thickness is presented elsewhere.[31] For completeness, we generalize previously derived mean-field expressions for the van der Waals parameter[31] $a(L)$ and the packing fraction[32] $\eta(\rho,L)$ so that they are also valid for films of arbitrary thickness.

A1. Cohesive Energy between Film Particles. Schoen and Diestler[31] have derived an expression for the effective van der Waals $a(L)$ parameter for a thin film confined between parallel walls, which we generalize for the present theory. Their derivation is only valid for films with $L = s_z - 2\sigma_{fw} > 2\sigma_f$. Here, we present expressions for $a(L)$ that are valid for any film thickness $L > 0$.

In Schoen and Diestler's model, s_z is the distance between the planes of "wall" particle centers on the opposite surface layers of the parallel substrates, σ_f is the effective film particle diameter, σ_w is the effective wall particle diameter, and $\sigma_{fw} = (\sigma_f + \sigma_w)/2$. As in our theory, they make the assumption that the substrate walls are smooth so that $L = s_z - 2\sigma_{fw}$ represents the film thickness accessible to the particle centers. The reader is referred to their original paper for more details. In the present theory, we take all of these diameters to be equal to the soft-sphere diameter of the film particles, $\sigma_f = \sigma_w = \sigma_{fw} = \sigma_{SS}$, which we also take to be our length scale for nondimensionalization. However, to maintain generality, we show the full dimensional integration limits in Schoen and Diestler's notation for all expressions in this Appendix.

To obtain an analytical expression for $a(L)$, one simply integrates a model for pair attractions between particles u_{ff} over the equilibrium pair separations consistent with the space available to the particle centers:

$$a = \frac{1}{2V}\int_V d\mathbf{r}_1 \int_V d\mathbf{r}_2 \, g(r_{12}) \, u_{ff}(r_{12}) \tag{25}$$

where $V = A(s_z - 2\sigma_{fw}) = AL$ (see Figure 1). We use the following approximation for the radial distribution function $g(r_{12})$

$$g(r_{12}) = \begin{cases} 0 & |\mathbf{r}_2 - \mathbf{r}_1| < \sigma_f \\ 1 & |\mathbf{r}_2 - \mathbf{r}_1| \geq \sigma_f \end{cases} \tag{26}$$

thus effectively ignoring any effect of weak attractive interactions on the film structure. The attractive component of the standard Lennard-Jones potential is employed here $u_{ff} = -4\epsilon_f\sigma_f^6/r_{12}^6$. The integral in eq 25 is readily rewritten in cylindrical coordinates and $a(L)$ is given by[31]

$$a(L) = \frac{4\pi\epsilon_f\sigma_f^6}{s_z - 2\sigma_{fw}}\int_{\sigma_{fw}}^{s_z - \sigma_{fw}} dz_1 \left\{\int dz \int dr \, r(z^2 + r^2)^{-3}\right\}_{V(z_1)} \tag{27}$$

For the case, $L < \sigma_f$, excluded volume considerations allow the integral in eq 27 to be rewritten as

$$a = \frac{4\pi\epsilon_f\sigma_f^6}{s_z - 2\sigma_{fw}}\int_{\sigma_{fw}}^{s_z - \sigma_{fw}} dz_1 \int_{\sigma_{fw}}^{s_z - \sigma_{fw} - z_1} dz \int_{\sqrt{\sigma_f^2 - z^2}}^{\infty}\frac{r}{(z^2 + r^2)^3} dr$$

$$= \pi\epsilon_f\sigma_f^2 L = \frac{3}{8}\frac{L}{\sigma_f}a_b \qquad L < \sigma_f \tag{28}$$

where $a_b = 8\pi\epsilon_f\sigma_f^3/3$ is the "bulk" van der Waals parameter. For pore widths, $\sigma_f \leq L \leq 2\sigma_f$, the van der Waals parameter is conveniently written as a sum of three terms, $a = a_1 + a_2 + a_3$, and the individual contributions are given by

$$a_1 = a_3 = \frac{4\pi\epsilon_f\sigma_f^6}{s_z - 2\sigma_{fw}}\int_{\sigma_{fw}}^{s_z - \sigma_{fw} - \sigma_f} dz_1$$

$$\left[\int_{\sigma_{fw} - z_1}^{\sigma_f} dz \int_{\sqrt{\sigma_f^2 - z^2}}^{\infty}\frac{r}{(z^2 + r^2)^3} dr + \int_{\sigma_f}^{s_z - \sigma_{fw} - z_1} dz \int_0^{\infty}\frac{r}{(z^2 + r^2)^3} dr\right]$$

$$a_2 =$$

$$\frac{4\pi\epsilon_f\sigma_f^6}{s_z - 2\sigma_{fw}}\int_{s_z - \sigma_{fw} - \sigma_f}^{\sigma_{fw} - \sigma_f} dz_1 \int_{\sigma_{fw} - z_1}^{s_z - \sigma_{fw} - z_1} dz \int_{\sqrt{\sigma_f^2 - z^2}}^{\infty}\frac{r}{(z^2 + r^2)^3} dr \tag{29}$$

The result for the above expression is identical to that derived by Schoen and Diestler for larger pore sizes,[31] $L \geq 2\sigma_f$, and it is given by

$$a = \frac{8\pi\epsilon_f\sigma_f^3}{3}\left[1 - \frac{3\sigma_f}{4L} + \frac{\sigma_f^3}{8L^3}\right] = a_b\left[1 - \frac{3\sigma_f}{4L} + \frac{\sigma_f^3}{8L^3}\right]$$

$$L \geq \sigma_f \tag{30}$$

We use nondimensionalized versions of eq 28 and 30 with $\sigma_f = \sigma_{SS}$ for the SSMF film theory of section II (see eq 13).

A2. Packing Fraction in the Thin-Film Geometry. Truskett et al.[32] derived a mean-field expression for the packing fraction $\eta(\rho,L)$ of spherical particles in a slit-pore geometry averaged over the volume $V = AL$ accessible to their centers. Their calculation produced an equation valid for $L > \sigma_f/2$, where again we have adopted Schoen and Diestler's notation[31] used in Appendix A1. Here we extend the derivation of Truskett et al. so that the relationship for $\eta(\rho,L)$ is valid for arbitrary film thickness $L > 0$.

The nonuniform spatial distribution of the local packing fraction in a thin-film geometry $\eta_{loc}(z)$ is simply the probability that a randomly chosen point on the plane of area A centered at vertical position z lies within a distance $\sigma_f/2$ of a particle center. The local packing fraction $\eta_{loc}(z)$ can be determined by integrating over the area of intersection $A^{int}(z,z') = \pi[(\sigma_f/2)^2 - (z - z')^2]$ between each sphere centered at z' and the plane at z. The average packing fraction $\eta(\rho,L)$ is calculated by integrating the $\eta_{loc}(z)$ over the volume accessible to the sphere centers. Truskett et al.[32] derived the following result valid for $L \geq \sigma_f/2$

$$\eta_{loc}(z) = \int_{z-\sigma_f/2}^{z+\sigma_f/2} dz' \, \rho(z') \, A^{int}(z,z')$$

$$\eta(\rho,L) = (s_z - 2\sigma_{fw})^{-1} \int_{\sigma_{fw}}^{s_z-\sigma_{fw}} dz \, \eta_{loc}(z)$$

$$= \frac{\pi\sigma_f^3 \rho}{6} - \frac{2}{s_z - 2\sigma_{fw}} \int_{\sigma_w/2}^{\sigma_{fw}} dz \, \eta_{loc}(z) \quad (31)$$

The integration limits are slightly different for films of thickness $L < \sigma_f/2$,

$$\eta(\rho,L) = \frac{\pi\sigma_f^3 \rho}{6} - \frac{2}{s_z - 2\sigma_{fw}} [\int_{\sigma_w/2}^{s_z-\sigma_{fw}-\sigma_f/2} dz \times$$

$$\int_{\sigma_{fw}}^{z+\sigma_f/2} dz' \, \rho(z') \, A^{int}(z,z') +$$

$$\int_{s_z-\sigma_{fw}-\sigma_f/2}^{\sigma_{fw}} dz \int_{\sigma_{fw}}^{s_z-\sigma_{fw}} dz' \, \rho(z') \, A^{int}(z,z')] \quad (32)$$

In the case of a uniform number density profile, i.e., a mean-field approximation for the spatial distribution of particles, we can integrate the above expressions to determine the confinement-induced changes to the average packing fraction $\eta(\rho,L)$:

$$\eta(\rho,L) = \begin{cases} \left(\dfrac{\pi\sigma_f^3 \rho}{6}\right)\left(\dfrac{3L}{2\sigma_f} - \dfrac{L^3}{\sigma_f^3}\right) & L < \sigma_f/2 \\[2mm] \left(\dfrac{\pi\sigma_f^3 \rho}{6}\right)\left(1 - \dfrac{3\sigma_f}{16L}\right) & L \geq \sigma_f/2 \end{cases} \quad (33)$$

We use nondimensionalized versions of these expressions with $\sigma_f = \sigma_{SS}$ for the SSMF film theory of section II (see eq 14).

Appendix B: Calculating the IG Transition Temperature

What is the basic procedure for determining the IG transition temperature of the film? First, note that the IG transition temperature of the bulk system $T_b^{IG}(p_b)$ at pressure p_b is formally defined by the relation $T_b^{IG}(p_b) = T^{IG}[L\rightarrow\infty,\rho_b^{IG}(p_b)]$ given by eq 18, where the bulk density $\rho_b^{IG}(p_b) = \rho_b(p_b,T_b^{IG})$ is obtained by inverting the equation of state $p_b = p^{\parallel}(L\rightarrow\infty,\rho_b, T_b^{IG})$. Similarly, the IG transition temperature of the model film in equilibrium with the bulk phase at pressure p_b, which we write as $T^{IG}(L,p_b) = T^{IG}[L,\rho^{IG}(L,p_b)]$, is obtained from eq 18, but now the film density $\rho^{IG}(L,p_b) \equiv \rho(L,p_b,T^{IG})$ is fixed by the condition that the film and the bulk phase must satisfy equality of chemical potentials; i.e., $\mu[L\rightarrow\infty,\rho_b(p_b,T^{IG}),T^{IG}] = \mu[L,\rho,T^{IG}]$. If eq 18 and the above constraints are linearized in the parameter L^{-1}, then one can obtain an analytical "thick-film" perturbation expression[35] for the shift in the IG transition $\Delta T^{IG}/T_b^{IG} = (T^{IG} - T_b^{IG})/T_b^{IG}$. Alternatively, one can use basic numerical techniques to solve for the values of T^{IG} and ρ^{IG} that satisfy eq 18 and the equilibrium conditions described above for arbitrary film thickness.

Appendix C: Energy Landscape Derived Pressure Tensor

The components of the pressure tensor for the SSMF film model can be derived by substituting eq 21 into eq 7. Here, we present analytical expressions valid for the fluid, i.e., $\beta < \beta^{IG}$:

$$p^{\parallel} = \frac{n}{3}\left(1 - \frac{3}{16L}\right)^{n/3} \rho^{n/3+1}\left[\gamma_{\infty} - \frac{[\gamma_{\infty} - \gamma_m]^2}{2\sigma_{\infty}}\beta\rho^{n/3} \times\right.$$

$$\left.\left(1 - \frac{3}{16L}\right)^{n/3}\right] + \frac{n+2}{2\beta}\rho - a_b\left[1 - \frac{3}{4L} + \frac{1}{8L^3}\right]\rho^2$$

$$0 < L^{-1} < 1$$

$$= \frac{n}{3}\left(1 - \frac{3}{16L}\right)^{n/3} \rho^{n/3+1}\left[\gamma_{\infty} - \frac{[\gamma_{\infty} - \gamma_m]^2}{2\sigma_{\infty}}\beta\rho^{n/3} \times\right.$$

$$\left.\left(1 - \frac{3}{16L}\right)^{n/3}\right] + \frac{n+2}{2\beta}\rho - \frac{3}{8}a_b L\rho^2 \quad 1 < L^{-1} < 2$$

$$= \frac{n}{3}\left(\frac{3}{2}L - L^3\right)^{n/3} \rho^{n/3+1}\left[\gamma_{\infty} - \frac{[\gamma_{\infty} - \gamma_m]^2}{2\sigma_{\infty}}\beta\rho^{n/3} \times\right.$$

$$\left.\left(\frac{3}{2}L - L^3\right)^{n/3}\right] + \frac{n+2}{2\beta}\rho - \frac{3}{8}a_b L\rho^2 \quad 2 < L^{-1} < \infty \quad (34)$$

and

$$p^{\perp} = \frac{n}{3}\left(1 - \frac{3}{8L}\right)\left(1 - \frac{3}{16L}\right)^{n/3-1} \rho^{n/3+1}\left[\gamma_{\infty} - \frac{[\gamma_{\infty} - \gamma_m]^2}{2\sigma_{\infty}} \times\right.$$

$$\left.\beta\rho^{n/3}\left(1 - \frac{3}{16L}\right)^{n/3}\right] + \frac{n+2}{2\beta}\frac{(1 - 3/(8L))}{(1 - 3/(16L))}\rho -$$

$$a_b\left[1 - \frac{3}{2L} + \frac{1}{2L^3}\right] - \Psi_0\rho\left[\frac{1 + 3(1/L)}{L(1 + (1/L))^3}\right] \quad 0 < L^{-1} < 1$$

$$= \frac{n}{3}\left(1 - \frac{3}{8L}\right)\left(1 - \frac{3}{16L}\right)^{n/3-1} \rho^{n/3+1}\left[\gamma_{\infty} - \frac{[\gamma_{\infty} - \gamma_m]^2}{2\sigma_{\infty}} \times\right.$$

$$\left.\beta\rho^{n/3}\left(1 - \frac{3}{16L}\right)^{n/3}\right] + \frac{n+2}{2\beta}\frac{(1 - 3/(8L))}{(1 - 3/(16L))}\rho -$$

$$\Psi_0\rho\left[\frac{1 + 3(1/L)}{L(1 + (1/L))^3}\right] \quad 1 < L^{-1} < 2$$

$$= \frac{2n}{3}L^3\left(\frac{3}{2}L - L^3\right)^{n/3-1} \rho^{n/3+1}\left[\gamma_{\infty} - \frac{[\gamma_{\infty} - \gamma_m]^2}{2\sigma_{\infty}}\beta\rho^{n/3} \times\right.$$

$$\left.\left(\frac{3}{2}L - L^3\right)^{n/3}\right] + \frac{n+2}{2\beta}\frac{2L^2}{(3/2 - L^2)}\rho - \Psi_0\rho\left[\frac{1 + 3(1/L)}{L(1 + (1/L))^3}\right]$$

$$2 < L^{-1} < \infty \quad (35)$$

In the above, $\gamma_{\infty} = y_{\infty}(\pi/6)^{n/3}$ and $\gamma_{min} = y_{min}(\pi/6)^{n/3}$.

The inherent structure contributions to the pressure tensor $p_{IS}^{\parallel}$ and $p_{IS}^{\perp}$ are defined by eqs 8 and , respectively (for more details, see ref 23). Here we present expressions for these quantities valid for the SSMF film in the infinite temperature limit. In other words, what follows are the components of the inherent structure pressure tensor that would be obtained from rapidly quenching a high-temperature fluid film,

$$p_{IS}^{\parallel} = \frac{n}{3}\gamma_{\infty}\left(1 - \frac{3}{16L}\right)^{n/3} \rho^{n/3+1} - a_b\rho^2\left[1 - \frac{3}{4L} + \frac{1}{8L^3}\right]$$

$$0 < L^{-1} < 1$$

$$= \frac{n}{3}\gamma_{\infty}\left(1 - \frac{3}{16L}\right)^{n/3} \rho^{n/3+1} - \frac{3}{8}a_b L\rho^2 \quad 1 < L^{-1} < 2$$

$$= \frac{n}{3}\gamma_{\infty}\left(\frac{3}{2}L - L^3\right)^{n/3} \rho^{n/3+1} - \frac{3}{8}a_b L\rho^2 \quad 2 < L^{-1} < \infty \quad (36)$$

Predicting the Properties of Thin Films

J. Phys. Chem. B, Vol. 108, No. 51, 2004 **19779**

and

$$p_{IS}^{\perp} = \frac{n}{3}\gamma_{\infty}\left(1 - \frac{3}{8L}\right)\left(1 - \frac{3}{16L}\right)^{n/3-1}\rho^{n/3+1} - a_b\rho^2\left[1 - \frac{3}{2L} + \right.$$
$$\left. \frac{1}{2L^3}\right] - \Psi_0\rho\left(\frac{1 + 3(1/L)}{L(1 + (1/L))^3}\right) \qquad 0 < L^{-1} < 1$$

$$= \frac{n}{3}\gamma_{\infty}\left(1 - \frac{3}{8L}\right)\left(1 - \frac{3}{16L}\right)^{n/3-1}\rho^{n/3+1} - $$
$$\Psi_0\rho\left(\frac{1 + 3(1/L)}{L(1 + (1/L))^3}\right) \qquad 1 < L^{-1} < 2$$

$$= \frac{2n}{3}\gamma_{\infty}L^3\left(\frac{3}{2}L - L^3\right)^{n/3-1}\rho^{n/3+1} - $$
$$\Psi_0\rho\left(\frac{1 + 3(1/L)}{L(1 + (1/L))^3}\right) \quad 2 < L^{-1} < \infty \quad (37)$$

The minimum condition for the transverse component of the inherent structure pressure $(\partial p_{IS}^{\parallel}/\partial\rho)_L = 0$ gives the transverse Sastry density $\rho_S^{\parallel}$:

$$\rho_S^{\parallel} = \left(\frac{2a_b\left(1 - \frac{3}{4L} + \frac{1}{8L^3}\right)}{\frac{n}{3}\left(\frac{n}{3} + 1\right)\gamma_{\infty}\left(1 - \frac{3}{16L}\right)^{n/3}}\right)^{1/(n/3-1)} \qquad 0 < L^{-1} < 1$$

$$= \left(\frac{\frac{3}{4}a_bL}{\frac{n}{3}\left(\frac{n}{3} + 1\right)\gamma_{\infty}\left(1 - \frac{3}{16L}\right)^{n/3}}\right)^{1/(n/3-1)} \qquad 1 < L^{-1} < 2$$

$$= \left(\frac{\frac{3}{4}a_bL}{\frac{n}{3}\left(\frac{n}{3} + 1\right)\gamma_{\infty}\left(\frac{3}{2}L - L^3\right)^{n/3}}\right)^{1/(n/3-1)} \qquad 2 < L^{-1} < \infty \quad (38)$$

A similar differentiation gives the following expressions that can be solved to determine the normal Sastry density $\rho_S^{\perp}$

$$\frac{n}{3}\left(\frac{n}{3} + 1\right)\gamma_{\infty}\left(1 - \frac{3}{8L}\right)\left(1 - \frac{3}{16L}\right)^{n/3-1}(\rho_S^{\perp})^{n/3} - $$
$$2a_b\left(1 - \frac{3}{2L} + \frac{1}{2L^3}\right)\rho_S^{\perp} - \Psi_0\left(\frac{1 + 3(1/L)}{L(1 + (1/L))^3}\right) = 0$$
$$0 < L^{-1} < 1$$

$$\frac{n}{3}\left(\frac{n}{3} + 1\right)\gamma_{\infty}\left(1 - \frac{3}{8L}\right)\left(1 - \frac{3}{16L}\right)^{n/3-1}(\rho_S^{\perp})^{n/3} - $$
$$\Psi_0\left(\frac{1 + 3(1/L)}{L(1 + (1/L))^3}\right) = 0 \qquad 1 < L^{-1} < 2$$

$$\frac{n}{3}\left(\frac{n}{3} + 1\right)\gamma_{\infty}2L^3\left(\frac{3L}{2} - L^3\right)^{n/3-1}(\rho_S^{\perp})^{n/3} - \Psi_0\left(\frac{1 + 3(1/L)}{L(1 + (1/L))^3}\right) = $$
$$0 \qquad 2 < L^{-1} < \infty \quad (39)$$

Using eq 38 and (39), we can construct a piecewise continuous and differentiable $\rho_S^{\perp} = \rho_S^{\parallel}$ curve in in the $(\Psi_0/a_b) - L^{-1}$ plane (see Figure 5).

References and Notes

(1) Gelb, L. D.; Gubbins, K. E.; Radhakrishnan, R.; Sliwinska-Bartkowiak, M. *Rep. Prog. Phys.* **1999**, *62*, 1573.

(2) Forrest, J. A.; Dalnoki-Veress, K. *Adv. Colloid Interface Sci.* **2001**, *94*, 167.

(3) McKenna, G. B. *J. Phys. IV (Fr.)* **2000**, *10*, Pr7−53.

(4) Wang, L.-M.; He, F.; Richert, R. *Phys. Rev. Lett.* **2004**, *92*, 095701.

(5) Jones, R. A. L. *Curr. Opin. Colloid Interface Sci.* **1999**, *4*, 153.

(6) Mischler, C.; Baschnagel, J.; Binder, K. *Adv. Colloid Interface Sci.* **2001**, *94*, 197.

(7) Drake, J. M.; Klafter, J. *Phys. Today* **1990**, *43*, 46.

(8) Creton, C.; Kramer, E. J.; Brown, H. R.; Hui, C. Y. *Adv. Polym. Sci.* **2001**, *156*, 53.

(9) Böhme, T. R.; de Pablo, J. J. *J. Chem. Phys.* **2002**, *116*, 9939. Fryer, D. S.; Nealey, P. F.; de Pablo, J. J. *Macromolecules* **2000**, *33*, 3376. Torres, J. A.; Nealey, P. F.; de Pablo, J. J. *Phys. Rev. Lett.* **2000**, *85*, 3221. Jain, T.; de Pablo, J. J. *Phys. Rev. Lett.* **2004**, *92*, 155505.

(10) Chou, S. Y.; Krauss, P. R.; Renstrom, P. J. *J. Vac. Sci. Technol. B* **1996**, *14*, 4129. Xia, Y.; Whitesides, G. M. *Angew. Chem., Int. Ed. Engl.* **1998**, *37*, 550. Colburn, M.; Johnson, S.; Damle, S.; Bailey, T.; Choi, B.; Wedlake, M.; Michaelson, T.; Sreenivasan, S. V.; Ekerdt, J.; Willson, C. G. *Proc. SPIE Int. Soc. Opt. Eng.* **1999**, *3676*, 379. Hutchinson, J. W.; Evans, A. G. *ACTA Materialia* **2000**, *48*, 125. Tanaka, T.; Morigami, M.; Atoda, N. *Jpn. J. Appl. Phys.* **1993**, *32*, 6059.

(11) Stillinger, F. H.; Weber, T. A. *Phys. Rev. A* **1982**, *25*, 978.

(12) Goldstein, M. *J. Chem. Phys.* **1969**, *51*, 3728.

(13) Stillinger, F. H. *Science* **1995**, *267*, 1935.

(14) Debenedetti, P. G.; Stillinger, F. H.; Truskett, T. M.; Roberts, C. J. *J. Phys. Chem. B* **1999**, *103*, 7390.

(15) Debenedetti, P. G.; Truskett, T. M.; Lewis, C. P.; Stillinger, F. H. *Adv. Chem. Eng.* **2001**, *28*, 21.

(16) Angelani, L.; Ruocco, G.; Sampoli, M.; Sciortino, F. *J. Chem. Phys.* **2003**, *119*, 2120. Shah, P.; Chakravarty, C. *Phys. Rev. Lett.* **2002**, *88*, 255501.

(17) Errington, J. R.; Debenedetti, P. G.; Torquato, S. *J. Chem. Phys.* **2003**, *118*, 2256.

(18) Corti, D. S.; Debenedetti, P. G.; Sastry, S.; Stillinger, F. H. *Phys. Rev. E* **1997**, *55*, 5522.

(19) Kauzmann, W. *Chem. Rev.* **1948**, *43*, 219. Gibbs, J. H.; Dimarzio, E. A. *J. Chem. Phys.* **1958**, *28*, 373. Kirkpatrick, T. R.; Wolynes, P. G. *Phys. Rev. B* **1987**, *36*, 8552. Stillinger, F. H. *J. Chem. Phys.* **1988**, *88*, 7818. Mézard, M.; Parisi, G. *Phys. Rev. Lett.* **1999**, *82*, 747.

(20) Stillinger, F. H.; Debenedetti, P. G.; Truskett, T. M. *J. Phys. Chem. B* **2001**, *105*, 11809.

(21) Diestler, D. J.; Schoen, M. *Acta Chim. Hung.* **1995**, *132*, 45.

(22) La Nave, E.; Sciortino, F.; Tartaglia, P.; Shell, M. S.; Debenedetti, P. G. *Phys. Rev. E* **2003**, *68*, 032103.

(23) Shell, M. S.; Debenedetti, P. G.; La Nave, E.; Sciortino, F. *J. Chem. Phys* **2003**, *118*, 8821. Debenedetti, P. G.; Stillinger, F. H.; Shell, M. S. *J. Phys. Chem. B* **2003**, *107*, 14434. Shell, M. S.; Debenedetti, P. G. *Phys. Rev. E* **2004**, *69*, 051102.

(24) LaViolette, R. A. *Phys. Rev. B* **1989**, *40*, 9952.

(25) Sastry, S.; Debenedetti, P. G.; Stillinger, F. H. *Phys. Rev. E* **1997**, *56*, 5533.

(26) Roberts, C. J.; Debenedetti, P. G.; Stillinger, F. H. *J. Phys. Chem. B* **1999**, *46*, 10258.

(27) Utz, M.; Debenedetti, P. G.; Stillinger, F. H. *J. Chem. Phys.* **2001**, *114*, 10049.

(28) Shen, V. K.; Debenedetti, P. G.; Stillinger, F. H. *J. Phys. Chem. B* **2002**, *106*, 10447.

(29) Sastry, S.; Debenedetti P. G.; Stillinger, F. H. *Nature* **1998**, *393*, 554.

(30) Hoover, W. G.; Ross, M. *Contemp. Phys.* **1971**, *12*, 339.

(31) Schoen, M.; Diestler, D. J. *J. Chem. Phys.* **1998**, *109*, 5596.

(32) Truskett, T. M.; Debenedetti, P. G.; Torquato, S. *J. Chem. Phys.* **2001**, *114*, 2401.

(33) Scala, A.; Starr, F. W.; La Nave, E.; Sciortino, F.; Stanley, H. E. *Nature* **2000**, *406*, 166. Sastry, S. *Nature* **2001**, *409*, 164. Saika-Voivod, I.; Poole, P. H.; Sciortino, F. *Nature* **2001**, *412*, 514.

(34) Angelani, L.; Di Leonardo, R.; Ruocco, G.; Scala, A.; Sciortino, F. *Phys. Rev. Lett.* **2000**, *85*, 5356. La Nave E.; Mossa, S.; Sciortino, F. *Phys. Rev. Lett.* **2002**, *88*, 225701. Sastry, S. *J. Phys: Condens. Matter* **2000**, *12*, 6515.

(35) Truskett, T. M.; Ganesan, V. *J. Chem. Phys.* **2003**, *119*, 1897.

(36) Di Leonardo, R.; Angelani, L.; Parisi, G.; Ruocco, G. *Phys. Rev. Lett.* **2000**, *84*, 6054.

(37) McCoy J. D.; Curro, J. G. *J. Chem. Phys.* **2002**, *116*, 9154.

(38) Mao, S. X.; Han, X.; Wiezorek, J. M. *Philos. Mag.* **2003**, *83*, 1807.

(39) Gersappe, D.; Robbins, M. O. *Europhys. Lett.* **1999**, *48*, 150.

(40) Evans, R. *J. Phs.: Condens. Matter* **1990**, *2*, 8989.

(41) Sastry, S. *Phys. Rev. Lett.* **2000**, *85*, 590.

(42) Muller, E.; Hung, F.; Gubbins, K. E. *Langmuir* **2000**, *16*, 5418.